# High-Throughput Design of Biocompatible Enzyme-Based Hydrogel Microparticles with Autonomous Movement

Keller, Shauni; Teora, Serena P.; Hu, Guo Xun; Nijemeisland, Marlies; Wilson, Daniela A.

**DOI**
10.1002/ange.201805661

**Publication date**
2018

**Document Version**
Final published version

**Published in**
Angewandte Chemie - International Edition

Micromotors Hot Paper

Deutsche Ausgabe: DOI: 10.1002/ange.201805661
Internationale Ausgabe: DOI: 10.1002/anie.201805661

# High-Throughput Design of Biocompatible Enzyme-Based Hydrogel Microparticles with Autonomous Movement

*Shauni Keller, Serena P. Teora, Guo Xun Hu, Marlies Nijemeisland, and Daniela A. Wilson**

***Abstract:*** *Micro- and nanomotors and their use for biomedical applications have recently received increased attention. However, most designs use top-down methods to construct inorganic motors, which are labour-intensive and not suitable for biomedical use. Herein, we report a high-throughput design of an asymmetric hydrogel microparticle with autonomous movement by using a microfluidic chip to generate asymmetric, aqueous, two-phase-separating droplets consisting of poly(ethylene glycol) diacrylate (PEGDA) and dextran, with the biocatalyst placed in the PEGDA phase. The motor is propelled by enzyme-mediated decomposition of fuel. The speed of the motors is influenced by the roughness of the PEGDA surface after diffusion of dextran and was tuned by using higher molecular weight dextran. This roughness allows for easier pinning of oxygen bubbles and thus higher speeds of the motors. Pinning of bubbles occurs repeatedly at the same location, thereby resulting in constant circular or linear motion.*

Micromotors and nanomotors come in all shapes and sizes and have been designed for many different applications, from water remediation[1–3] and sensing,[4,5] to biomedical applications.[6–10] Until recently most of these motors were fabricated from inorganic materials, usually using top-down lithography methods.[1,11,12] However, top-down lithography is a very labour-intensive and expensive method and is difficult to scale-up, while the resulting motors are usually not biocompatible. In our view, a suitable design for biomedical applications should be inspired by nature, and thus it should be designed using a bottom-up method, it should be biodegradable, or at least biocompatible, should be driven by biocatalysts which provide access to biologically relevant fuels, and should provide a soft interface with biological systems. However, incorporating all these requirements in a motor design with control over the sizes and shapes remains a challenge.[13]

In our previous studies we used the self-assembly of amphiphilic block copolymers to design supramolecular nanomotors. The poly(ethylene glycol)-polystyrene polymers spontaneously self-assemble into polymersomes upon addition of water. Subsequent dialysis induces shape transformation into asymmetric structures, which are able to capture catalysts. Both an inorganic catalyst (platinum)[14] and biocatalysts (catalase and glucose oxidase) were used.[15,16] Although this is a bottom-up model designed to study the effect of motion in biological systems,[6,7] the hydrophobic polymer is not biodegradable. Further developments for drug-delivery applications should incorporate both biocompatible and biodegradable components.

Recent research has focused on biocatalysts and soft materials to provide a more adequate interface with biological systems. Enzymes have been immobilized on many inorganic structures, such as spheres,[17] tubes,[1,8,18] and hollow capsules. Catalase is commonly used as a biocatalyst, while other examples are glucose oxidase[15] and urea.[19] The soft materials investigated for use in the (bottom-up) assembly of motors are polymers, such as PDMS,[20,21] chitosan,[2,22] and poly(ethylene glycol) diacrylate (PEGDA).[23] The catalysts incorporated in most of these motors are inorganic materials, such as magnesium[2,10] or platinum.[21–25] Although these contain a soft component, the overall structure only provides access to limited types of fuels and shapes. Some attempts have been made to create biodegradable[5,8,26] or biocompatible[19,20] motors. Despite these attempts, surfactant is usually added to facilitate bubble propulsion. However, this is not possible in biological systems. The challenge remains to make soft, biocompatible motors using a biocatalyst produced by a method that allows for scaling-up. We propose a general solution to producing asymmetric motors by using biocompatible materials and biocatalysts.

Bottom-up assembly makes it possible to design soft structures in a simple way with high efficiency. Microfluidics provide an ideal application of such a self-assembly technique. Recent examples of micromotors obtained by microfluidics[3,22] show its major advantages over top-down methods are the high-throughput, easy handling, and versatility. Here we show the first high-throughput design of asymmetric, biocompatible micromotors through spontaneous phase separation of microfluidic droplets containing two immiscible aqueous phases. This general microfluidic design fabricates single-emulsion microdroplets containing two immiscible solutions dispersed in oil. The droplets then spontaneously phase-separate into droplet-in-droplet morphologies of controlled size, which upon polymerization leads to the desired asymmetrical gel particle.[27] The biocatalyst catalase, which is entrapped inside the hydrogel, decomposes hydrogen peroxide into water and oxygen bubbles and is responsible for the

[*] S. Keller, S. P. Teora, G. X. Hu, M. Nijemeisland, Prof. Dr. D. A. Wilson
Department Systems Chemistry
Institution Radboud University
Institute for Molecules and Materials
Heyendaalseweg 135, 6525 AJ, Nijmegen (The Netherlands)
E-mail: d.wilson@science.ru.nl
M. Nijemeisland
Current address: Faculty of Aerospace Engineering Novel Aerospace Material, Institution Tu Delft University (The Netherlands)
Supporting information and the ORCID identification number(s) for the author(s) of this article can be found under: https://doi.org/10.1002/anie.201805661.

  

propulsion of the micromotor (Figure 1). These new types of motors will be used to study different effects that influence motion, such as fuel concentration and surface roughness. This will be different for enzyme- and hydrogel-based motors

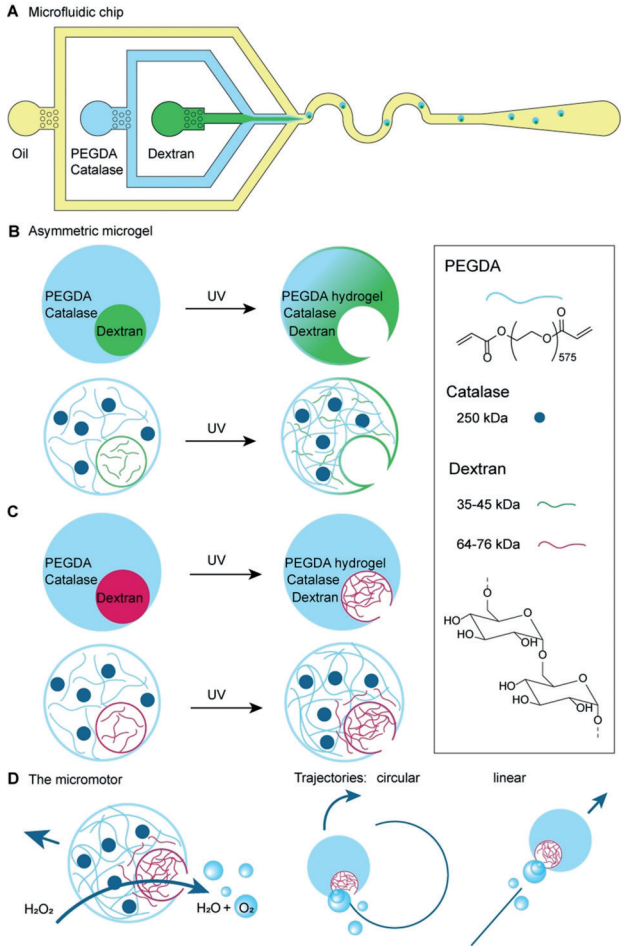


***Figure 1.*** Microfluidic design of asymmetric hydrogels. A) A microfluidic chip is used to construct ATPS droplets. There are three inlets—for oil, PEGDA, and dextran—and one outlet. At the first cross-junction, an ATPS jet is formed which is emulsified at the second cross-junction. B) Schematic depiction of the two-phase droplet and hydrogel made with low-molecular-weight and C) with high-molecular-weight dextran. D) Schematic representation of the resulting motor which converts hydrogen peroxide into water and propelling oxygen. The trajectory of the motor is either circular or linear, depending on where the bubbles pin.

than for inorganic motors. Inorganic motors usually increase speed as the fuel concentration increases.[28] However, enzymes show a different behavior, namely an optimum in activity depending on its environment. Catalase, for example, is inhibited by its own fuel when this is present in high concentrations.[29] Therefore, we expect to observe an optimum concentration of hydrogen peroxide at which these motors move the fastest. Surface roughness has also been shown previously to play an important role in pinning gas bubbles.[12] The easy generation of bubbles is of great importance for bubble-propelled motors. If bubbles are generated more easily, the motor will be propelled faster. Although the motor reported here is different in terms of materials and shape, we expect that surface roughness will affect its speed.

The microfluidic chip, which is made of polydimethyl sulfoxane (PDMS), consists of three inlets for oil, PEGDA, and dextran and one outlet to collect the microdroplets (Figure 1 A and Figure S1 in the Supporting Information). The first cross-junction gives rise to a two-phase jet consisting of dextran and PEGDA. At the second cross-junction the continuous oil phase emulsifies this jet into single-emulsion microdroplets. Subsequently, the droplets phase-separate and are collected at the outlet, after which the PEGDA phase is photocured. Upon polymerization, the dextran diffuses inside the PEGDA gel and leaves an opening behind.

To ensure a biocompatible design, we use catalase as the biocatalyst to provide the propelling force for the motors. The enzyme was dissolved in the PEGDA phase prior to injection into the microfluidic set-up, thereby allowing the polymer network to form around the catalyst upon polymerization of the PEGDA (Figure 1 B). Based on its design, homogeneous distribution of the enzyme throughout the hydrogel is expected and observed (Figure S2). After UV exposure, 52 % of the original catalase activity was preserved (Figure S3). To check whether the enzyme would stay inside the gel, inductively coupled plasma mass spectrometry measurements were performed on the supernatant of the sample over several days. This technique can determine low concentrations (down to parts per million) of elements in solution. Measurements performed on the element iron, which is present in the active site of catalase, did not show any correlation, thus demonstrating the enzyme is safely trapped inside the structures without leakage (Figure S4).

The dimensions of the microfluidic device and flow rates of all the phases allow for control and fine-tuning of the size of the droplets. The motors reported here are $(19.8 \pm 0.4)$ μm in diameter with an opening of $(8.2 \pm 0.5)$ μm. Furthermore, the size of the inner droplet can also be fine-tuned through the flow rate of the immiscible phase. This leads to asymmetric gel particles of different shapes with different sizes of "openings" (Figure S5). These particles nicely correlate in shape with our previous bowl-shaped stomatocyte nanomotors and allow further understanding of the mechanism of movement.

We hypothesized that surface roughness plays an important role in bubble-propelled motion. To investigate the influence of roughness on the speed of the motors we used low- and high-molecular-weight dextran (Figure 1 C). The low-molecular-weight dextran was able to diffuse inside the PEGDA hydrogel, while the high-molecular-weight dextran was not and induced roughness of the inner PEGDA surface. These scenarios were seen by fluorescence microscopy, where FITC-labelled low-molecular-weight dextran diffused into the PEGDA gel, while rhodamine B-labelled high-molecular-weight dextran remained in the opening of the microgel (Figure 2 A). Further characterization using cryo-scanning electron microscopy (cryo-SEM) demonstrated that this lack of diffusion by high-molecular-weight dextran induced surface roughness in the opening of the asymmetric gel (Figure 2 B). The batches made with low-molecular-weight dex-

  

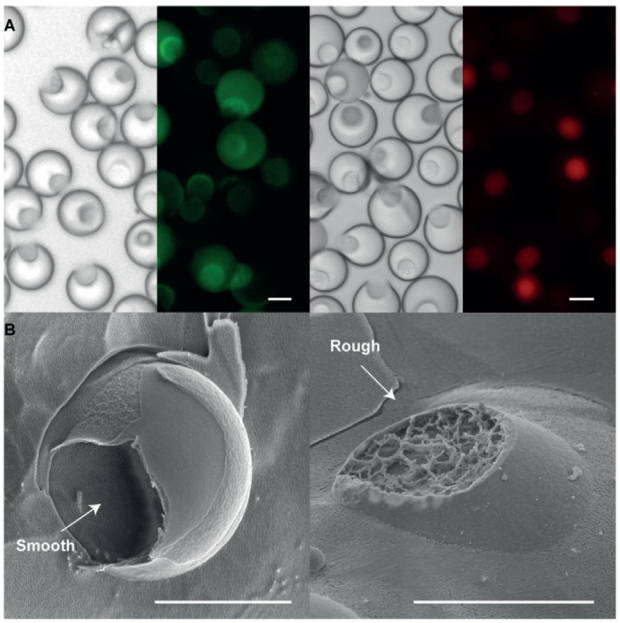


***Figure 2.*** Characterization of microgels by A) fluorescence microscopy with and B) cryo-SEM using FITC-labelled low-molecular weight dextran (left) and rhodamine B-labelled high-molecular-weight dextran (right). Scale bar: 10 μm. FITC = fluorescein-5-isothiocyanate.

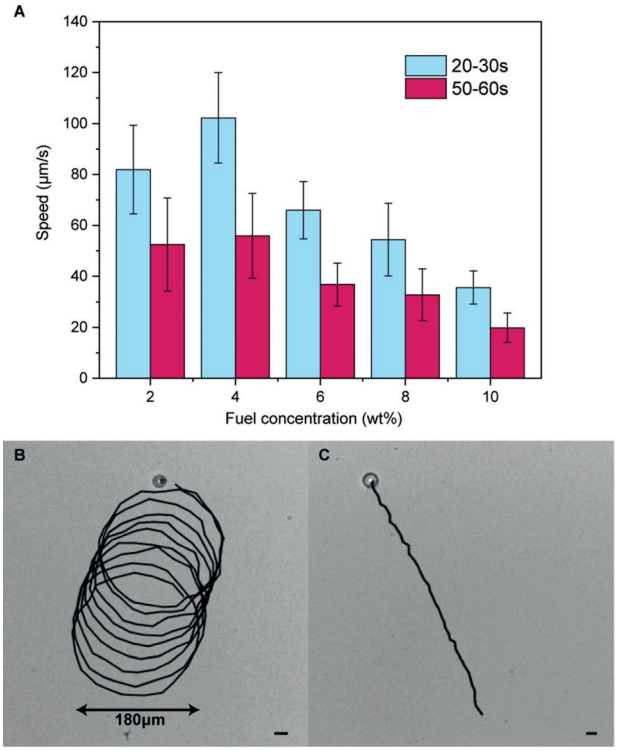


***Figure 3.*** A) Speed as a function of hydrogen peroxide concentration. B) Motors trajectories: constant movement of the micromotors in a circular (left) or linear (right) fashion. Scale bar: 20 μm.

tran showed differences in roughness because of partial diffusion of the dextran into the gel (Figure S6).

To analyze the speed of the micromotor, ten of the fastest motors were tracked for 10 s at two specific time points, namely at 20 s and at 50 s after addition to the fuel. From these measurements the average speed was calculated. Motors made using low-molecular-weight dextran showed differences in surface roughness. Since surface roughness influences the speed of motors by pinning bubbles, it also influences the speed of the motors. The high-molecular-weight system did not show this heterogeneity and thus we achieved better control over the speed. The speed of the motors was found to be dependent on the concentration of the fuel (Figure 3A), in this case hydrogen peroxide. We observed the highest speed at 4% hydrogen peroxide for both 20 s and 50 s after addition. At 20 s after addition, this corresponds to a speed of 5.2 body lengths per second. At higher concentrations of fuel, the speed decreased rapidly over time. This is due to the fast inhibition of the enzyme by its own fuel. When the motors are added to high concentrations of fuel, such as 10% hydrogen peroxide, they initially move at high speeds, and then slow down fast within the first seconds. A second addition of micromotors to the same fuel solution resulted in the same bubble-propelled movement as observed in the first addition. This demonstrates that the observed decrease in speed is not due to lack of fuel but rather to inactivation of the enzyme. We didn't observe any bubble propulsion at fuel concentrations lower than 2%.

The principle of the micromotors movement is bubble propulsion. The bubbles are clearly visible as they grow from the opening of the motor, which is remarkable since the catalyst is homogeneously dispersed throughout the bead. We would thus expect the fuel to be converted all over the motor. However, the bubbles are only able to grow in the opening of the motors. The only difference between the inside of the opening and outside of the motor is the surface roughness. As can be seen by cryo-SEM (Figure 2B), the outer surface is rather smooth while the surface in the opening is rough. Even in the smooth openings made with the lower-molecular-weight dextran, the surface has small rough spots. This roughness enables pinning of the bubbles, which explains why bubbles grow from the opening despite the homogeneous distribution of catalyst. Furthermore, oversaturation of oxygen is more easily reached in the enclosed space of the opening. The location where the bubble is pinned determines where the propelling force exhibits its energy. Most of the motors we observed move in a constant circular fashion (Figure 3B and Supplementary video 1), whereas only a few motors exhibited linear motion (Figure 3C and Supplementary video 2). Such remarkable behaviour is most probably due to the shape of the gel microparticles. The constant circular motion is due to the repeated pinning of bubbles at the same off-centre location, thereby resulting in propulsion of the motors constantly at the same angle. Linear motion is, in contrast, a consequence of the pining of the bubble in the central part of the opening, which explains why this is observed less often since it is statistically less probable.

In summary, we have reported the first enzyme-driven gel micromotor which is based on soft, biocompatible materials made through a high-throughput, spontaneous bottom-up assembly using microfluidics. We showed the versatility of this method and the possibility to tune the size, shape, and roughness of the gel microparticles. A rough surface made it

  

easier to pin bubbles and resulted in better control over the speed compared to motors with less-defined roughness. This asymmetric shape and roughness makde it possible to obtain motion with a homogeneously distributed catalyst, which is unique in the micromotor field. We observed bubble propulsion for fuel concentrations from 2% to an optimum at 4%, which resulted in high speeds of 5.2 body lengths per second. Another remarkable feature of these motors is that the bubble always pins at the same location, thereby resulting in a constant circular or linear motion. Although this micromotor is made from biocompatible materials, it runs on hydrogen peroxide, which is, of course, not biocompatible. Therefore, other sources of fuel need to be investigated in the future.

This microfluidic design can be used for any two immiscible solutions, one of which can be photopolymerized. This creates considerable potential for designing other soft and biocompatible structures. Furthermore, the spontaneous phase separation allows for precision over two parameters: the asymmetric shape of the controlled opening and the size. Another advantage is that the microfluidic design allows the production of these structures to be scaled up, which makes it easy to produce large batches of high monodispersity. This will offer new possibilities to investigate different effects on the motion, such as size, shape, and material composition of the particles, as well as catalyst distribution.

## Acknowledgements

We acknowledge financial support from the NWO Chemiche Wetenschappen VIDI Grant 723.015.001. We also acknowledge support from the Ministry of Education, Culture and Science (Gravitation program 024.001.035). S.P.T acknowledges support from the Erasmus program. We would like to thank Aigars Piruska (Institute for Molecules and Materials, Radboud University) for providing the silicon master and Sjoerd Postma for the synthesis of the SS01 surfactant used in the microfluidic set-up.

## Conflict of interest

The authors declare no conflict of interest.

**Keywords:** active microparticles · enzymes · hydrogels · microfluidics · micromotors

**How to cite:** *Angew. Chem. Int. Ed.* **2018**, *57*, 9814–9817
*Angew. Chem.* **2018**, *130*, 9962–9965

[1] D. Vilela, J. Parmar, Y. F. Zeng, Y. L. Zhao, S. Sanchez, *Nano Lett.* **2016**, *16*, 2860–2866.
[2] J. A. M. Delezuk, D. E. Ramirez-Herrera, B. E. F. de Avila, J. Wang, *Nanoscale* **2017**, *9*, 2195–2200.
[3] A. Q. Chen, X. H. Ge, J. Chen, L. Y. Zhang, J. H. Xu, *Lab Chip* **2017**, *17*, 4220–4224.
[4] L. M. Liu, Y. G. Dong, Y. Y. Sun, M. Liu, Y. J. Su, H. Zhang, B. Dong, *Nano Res.* **2016**, *9*, 1310–1318.
[5] M. Liu, Y. Y. Sun, T. P. Wang, Z. R. Ye, H. Zhang, B. Dong, C. Y. Li, *J. Mater. Chem. C* **2016**, *4*, 5945–5952.
[6] F. Peng, Y. F. Tu, A. Adhikari, J. C. J. Hintzen, D. Lowik, D. A. Wilson, *Chem. Commun.* **2017**, *53*, 1088–1091.
[7] F. Peng, Y. F. Tu, J. C. M. van Hest, D. A. Wilson, *Angew. Chem. Int. Ed.* **2015**, *54*, 11662–11665; *Angew. Chem.* **2015**, *127*, 11828–11831.
[8] Z. G. Wu, X. K. Lin, X. Zou, J. M. Sun, Q. He, *ACS Appl. Mater. Interfaces* **2015**, *7*, 250–255.
[9] K. D. Seo, B. K. Kwak, S. Sanchez, D. S. Kim, *IEEE Trans. NanoBiosci.* **2015**, *14*, 298–304.
[10] B. E. F. de Avila, P. Angsantikul, J. X. Li, M. A. Lopez-Ramirez, D. E. Ramirez-Herrera, S. Thamphiwatana, C. R. Chen, J. Delezuk, R. Samakapiruk, V. Ramez, M. Obonyo, L. Zhang, J. Wang , *Nat. Commun.* **2017**, *8*, 272.
[11] L. X. Hu, J. M. Miao, G. Gruber, *RSC Adv.* **2016**, *6*, 3399–3405.
[12] S. J. Wang, N. Wu, *Langmuir* **2015**, *31*, 249.
[13] J. Wang, *Nanomachines: Fundamentals and Applications*, Wiley, Hoboken, **2013**.
[14] D. A. Wilson, R. J. M. Nolte, J. C. M. van Hest, *Nat. Chem.* **2012**, *4*, 268–274.
[15] L. Abdelmohsen, M. Nijemeisland, G. M. Pawar, G. J. A. Janssen, R. J. M. Nolte, J. C. M. van Hest, D. A. Wilson, *ACS Nano* **2016**, *10*, 2652–2660.
[16] M. Nijemeisland, L. Abdelmohsen, W. T. S. Huck, D. A. Wilson, J. C. M. van Hest, *ACS Cent. Sci.* **2016**, *2*, 843–849.
[17] J. Simmchen, A. Baeza, D. Ruiz-Molina, M. Vallet-Regi, *Nanoscale* **2014**, *6*, 8907–8913.
[18] S. Sanchez, A. A. Solovev, Y. Mei, O. G. Schmidt, *J. Am. Chem. Soc.* **2010**, *132*, 13144–13145.
[19] X. Ma, X. Wang, K. Hahn, S. Sanchez, *ACS Nano* **2016**, *10*, 3597–3605.
[20] W. Xi, F. Kong, J. C. Yeo, L. T. Yu, S. Sonam, M. Dao, X. B. Gong, C. T. Lim, *Proc. Natl. Acad. Sci. USA* **2017**, *114*, 10590–10595.
[21] M. D. Su, M. Liu, L. M. Liu, Y. Y. Sun, M. T. Li, D. L. Wang, H. Zhang, B. Dong, *Langmuir* **2015**, *31*, 11914–11920.
[22] A. X. Lu, Y. J. Liu, H. Oh, A. Gargava, E. Kendall, Z. H. Nie, D. L. DeVoe, S. R. Raghavan, *ACS Appl. Mater. Interfaces* **2016**, *8*, 15676–15683.
[23] H. Ceylan, I. C. Yasa, M. Sitti, *Adv. Mater.* **2017**, *29*, 1605072.
[24] L. M. Liu, M. Liu, Y. G. Dong, W. Zhou, L. N. Zhang, Y. J. Su, H. Zhang, B. Dong, *J. Mater. Sci.* **2016**, *51*, 1496–1503.
[25] W. Gao, S. Sattayasamitsathit, J. Orozco, J. Wang, *Nanoscale* **2013**, *5*, 8909–8914.
[26] C. R. Chen, E. Karshalev, J. X. Li, F. Soto, R. Castillo, I. Campos, F. Z. Mou, J. G. Guan, J. Wang, *ACS Nano* **2016**, *10*, 10389–10396.
[27] S. Ma, J. Thiele, X. Liu, Y. Bai, C. Abell, W. T. S. Huck, *Small* **2012**, *8*, 2356–2360.
[28] L. S. Liu, T. Bai, Q. J. Chi, Z. Wang, S. Xu, Q. W. Liu, Q. Wang, *Micromachines* **2017**, *8*, 0.
[29] O. M. Lardinois, M. M. Mestdagh, P. G. Rouxhet, *Biochim. Biophys. Acta Protein Struct. Mol. Enzymol.* **1996**, *1295*, 222–238.

Manuscript received: May 16, 2018
Accepted manuscript online: June 19, 2018
Version of record online: July 5, 2018

  